Science Advances
AAAS

Supplementary Materials for

Hyperselective carbon membranes for precise high-temperature H_2 and CO_2 separation

Gaurav M. Iyer *et al.*

Corresponding author: Chen Zhang, czhang71@umd.edu

Sci. Adv. **11**, eadt7512 (2025)
DOI: 10.1126/sciadv.adt7512

This PDF file includes:

Supplementary Text
Figs. S1 to S11
Tables S1 to S5
References

Supplementary Text

S1. Materials

m-Phenylenediamine (MPD, 99%), sodium carbonate (≥99.5%, anhydrous), and tetrahydrofuran (THF, ≥99.0%, anhydrous with 250 ppm BHT as inhibitor) were obtained from Sigma Aldrich (St. Louis, MO). N-methylpyrrolidone (NMP, ≥99.0%), methanol (≥99.8%), and hexane (≥98.5%, mixture of isomers) were obtained from VWR International (Radnor, PA). Isophthaloyl chloride (IPC, ≥99.0%), terephthaloyl chloride (TPC, ≥99.0%), and N,N-dimethylacetamide (DMAc, ≥99.8%, anhydrous) were obtained from Fisher Scientific™ (Pittsburgh, PA). All chemicals were used without further purification. Pure gases (ultra-high purity) and gas mixtures (certified standard) were obtained from Airgas (Hyattsville, MD).

S2. Gas transport in carbon molecular sieve membranes

Gas permeability (P_j, j = A or B) is defined as the steady-state permeation flux (N_j) normalized by the trans-membrane partial pressure difference (Δp_j) and the membrane selective layer thickness (L)

$$P_j = \frac{N_j \times L}{\Delta p_j} \tag{S1}$$

The membrane selective layer thickness was calculated from CMS hollow fiber wall thickness taking into account the volume fraction of macrovoids, which was obtained from SEM images. Gas permeability is given in the unit of Barrer

$$1\ \text{Barrer} = 1 \times 10^{-10} \frac{cm^3(STP) \cdot cm}{cm^2 \cdot s \cdot cmHg}$$

The ideal selectivity ($\alpha_{A/B}$) is defined as

$$\alpha_{A/B} = \frac{P_A}{P_B} \tag{S2}$$

According to the sorption-diffusion theory, permeability P_j can be written as the product of transport diffusivity D_j (cm^2/s) and sorption coefficient S_j (cm^3[STP]/$cm^3 \cdot$cmHg)

$$P_j = D_j \times S_j \tag{S3}$$

The temperature dependence of D_j and S_j can be described by the Arrhenius equation and van't Hoff equation, respectively

$$D_j = D_{j0} \times exp\left(\frac{-E_D}{RT}\right) \tag{S4}$$

$$S_j = S_{j0} \times exp\left(\frac{-H_S}{RT}\right) \tag{S5}$$

where D_{j0} and S_{j0} are pre-exponential factors, E_D is diffusion activation energy (J/mol), H_S is heat of adsorption (J/mol), R is ideal gas constant (J/mol·K), and T is absolute temperature (K). Therefore, the temperature dependence of permeability is

$$P_j = P_{j0} \times exp\left(\frac{-E_P}{RT}\right) \tag{S6}$$

where P_{j0} is pre-exponential factor and E_P is apparent permeation activation energy (J/mol)

$$E_P = E_D + H_S \tag{S7}$$

Transport diffusivity can be calculated using the permeation time lag (θ, second) obtained from permeation plot

$$D_j = \frac{L^2}{6\theta} \tag{S8}$$

The selectivity under mixed-gas permeation was calculated by

$$\alpha = \frac{y_A / y_B}{x_A / x_B} \tag{S9}$$

where y_A and y_B are molar fractions of A and B in the permeate obtained from stabilized GC injections, x_A and x_B are molar fractions of A and B in the feed mixture.

S3. Modeling membrane separators for H_2 enrichment

The materials balance equations and boundary conditions are

$$\frac{dF_j}{dz} = -\pi DNQ_j(p_j - p_{js}) \tag{S10}$$

$$z = 0, F_j = F_{j0}$$

$$\frac{dF_{js}}{dz} = \pi DNQ_j(p_j - p_{js}) \tag{S11}$$

$$z = 0, F_{js} = 0$$

$$p_T = \sum_j p_j \tag{S12}$$

$$p_{Ts} = \sum_j p_{js} \tag{S13}$$

$$F_T = \sum_j F_j \tag{S14}$$

$$F_{Ts} = \sum_j F_{js} \tag{S15}$$

where F_j and F_{js} are molar flow rate (mol/s) of component j at the feed side and permeate side, F_T and F_{Ts} are total molar flow rate (mol/s) at the feed side and permeate side, p_j and p_{js} are partial pressure (bar) of component j at the feed side and permeate side, p_T and p_{Ts} are total pressure (bar) at the feed side and permeate side, D is hollow fiber membrane outer diameter (m), Q_j is membrane permeance (mol/[m^2·s·bar]) of component j, and N is the number of hollow fiber membranes. Isothermal operation, plug flow, and no pressure drop were assumed. Feed and permeate conditions are summarized in Table S3. The modeling was carried out for membrane separators that consist of membranes with H_2/CO_2 separation performance shown in Table S4. It was assumed that all three membranes had the same separation layer thickness (41 μm).

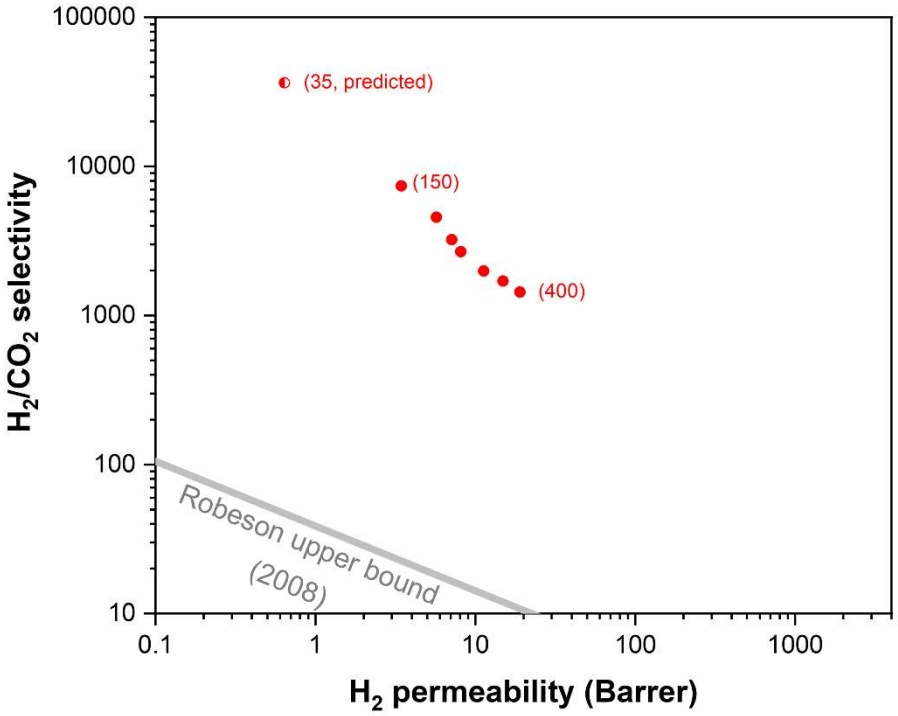


Fig. S1. Predicted mixed-gas H_2 permeabilities and H_2/CO_2 selectivities in the Aramid-1050 CMS membrane at permeation temperature of 35 °C (half-filled circle).

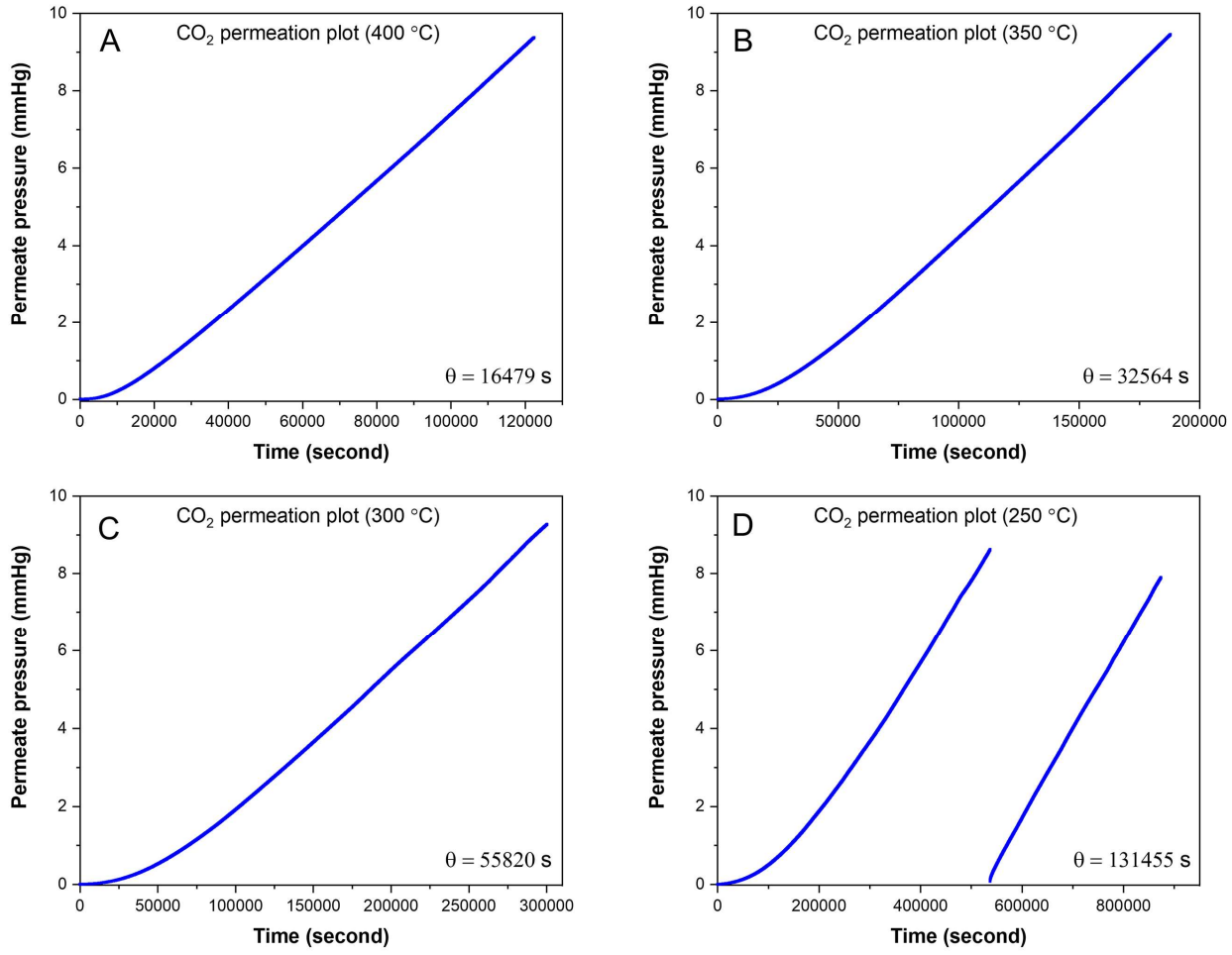


Fig. S2. Single-gas CO_2 permeation plots of the Aramid-1050 CMS membrane showing time lags at (A) 400 °C, (B) 350 °C, (C) 300 °C, and (D) 250 °C.

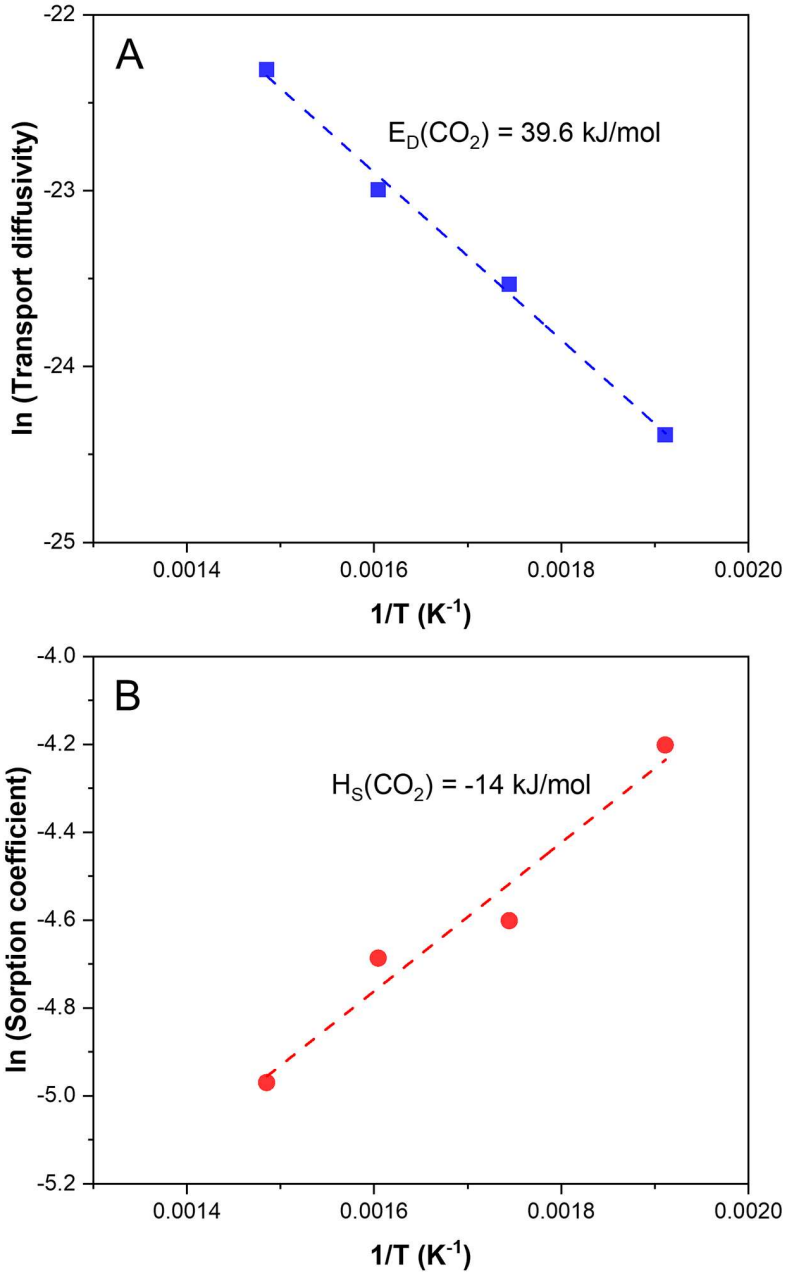


Fig. S3. Calculation of diffusion activation energy and heat of adsorption. (A) Arrhenius plot of CO_2 transport diffusivities in the Aramid-1050 CMS membrane at 250-400 °C. (B) van't Hoff plots of CO_2 sorption coefficients in the Aramid-1050 CMS membrane at 250-400 °C. The CO_2 transport diffusivities were calculated by the time-lag method using permeation time lags obtained from CO_2 permeation plots shown in Fig. S2. The CO_2 sorption coefficients were calculated by the sorption-diffusion theory using CO_2 transport diffusivities and single-gas CO_2 permeabilities (Fig. 1C).

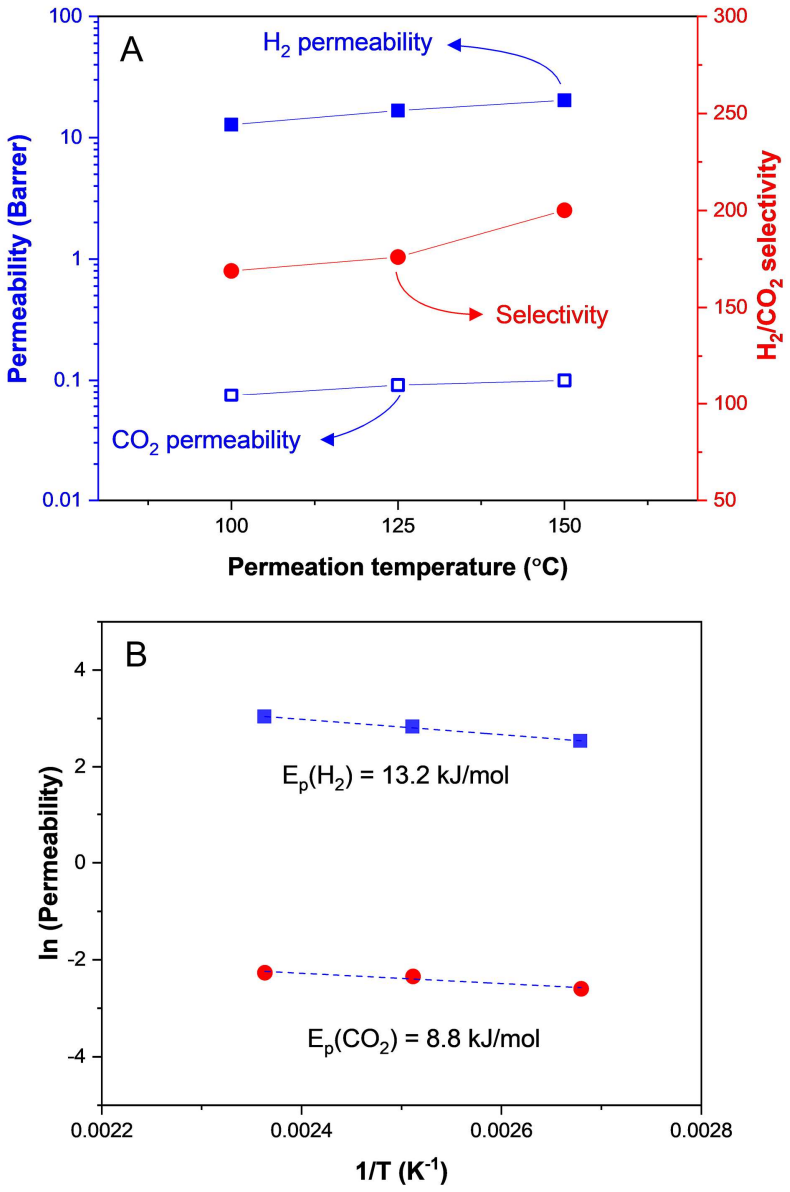


Fig. S4. H_2/CO_2 separation performance of the Aramid-925 CMS membrane. (A) H_2 permeability and H_2/CO_2 selectivity in the Aramid-925 CMS membrane. Permeation was carried out at 100, 125, and 150 °C using a 10%H_2/90%CO_2 mixture at 2 bar feed pressure. (B) Arrhenius plots of H_2 and CO_2 permeabilities showing permeation activation energies in the Aramid-925 CMS membrane.

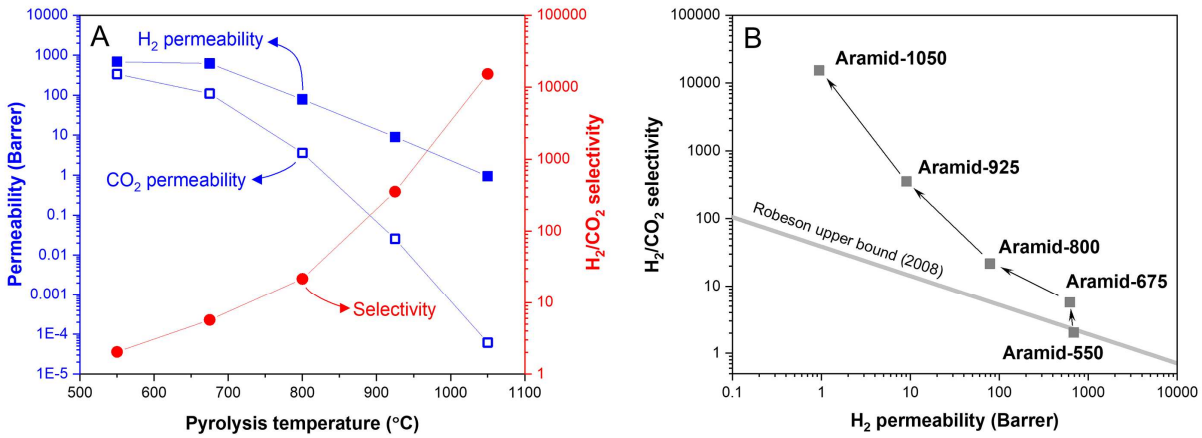


Fig. S5. H_2/CO_2 separation performance (35 °C) of aramid-derived CMS membranes pyrolyzed at 550 to 1050 °C. (A) The effects of pyrolysis temperature on H_2 permeability, CO_2 permeability, and H_2/CO_2 selectivity. (B) Comparing the H_2/CO_2 separation performance of aramid-derived CMS membranes with the 2008 Robeson upper bound. Separation performance of Aramid-550, Aramid-675, Aramid-800, and Aramid-925 CMS membranes were measured using single-gas permeation at 35 °C.*(17)* Separation performance of the Aramid-1050 CMS membrane at 35 °C was predicted using single-gas permeation data (Fig. 1C) measured at 250 to 400 °C and the Arrhenius equation.

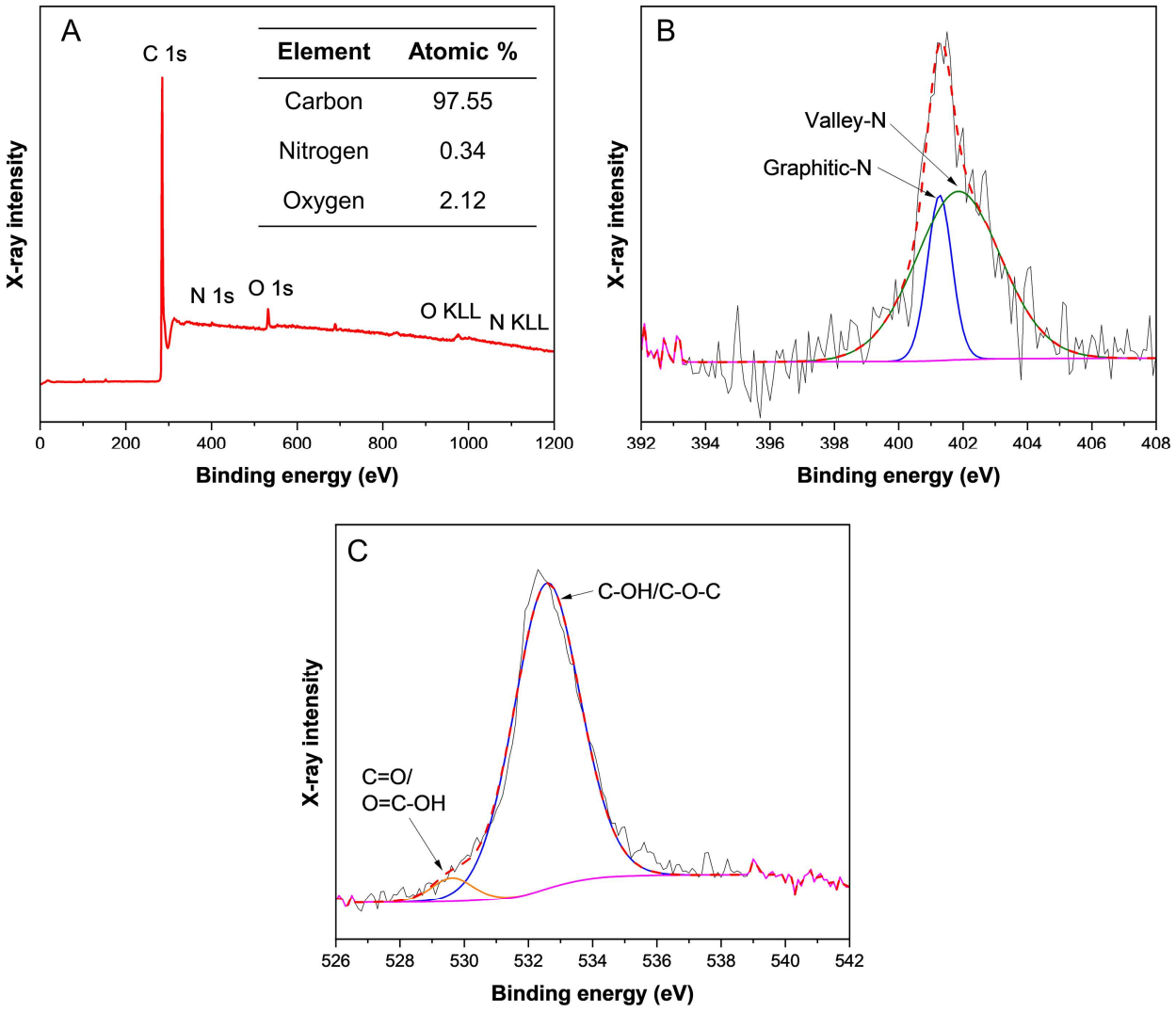


Fig. S6. XPS results in the Aramid-1050 CMS membrane. (A) XPS survey spectra. (B) High-resolution N1s spectra. (C) High-resolution O1s spectra.

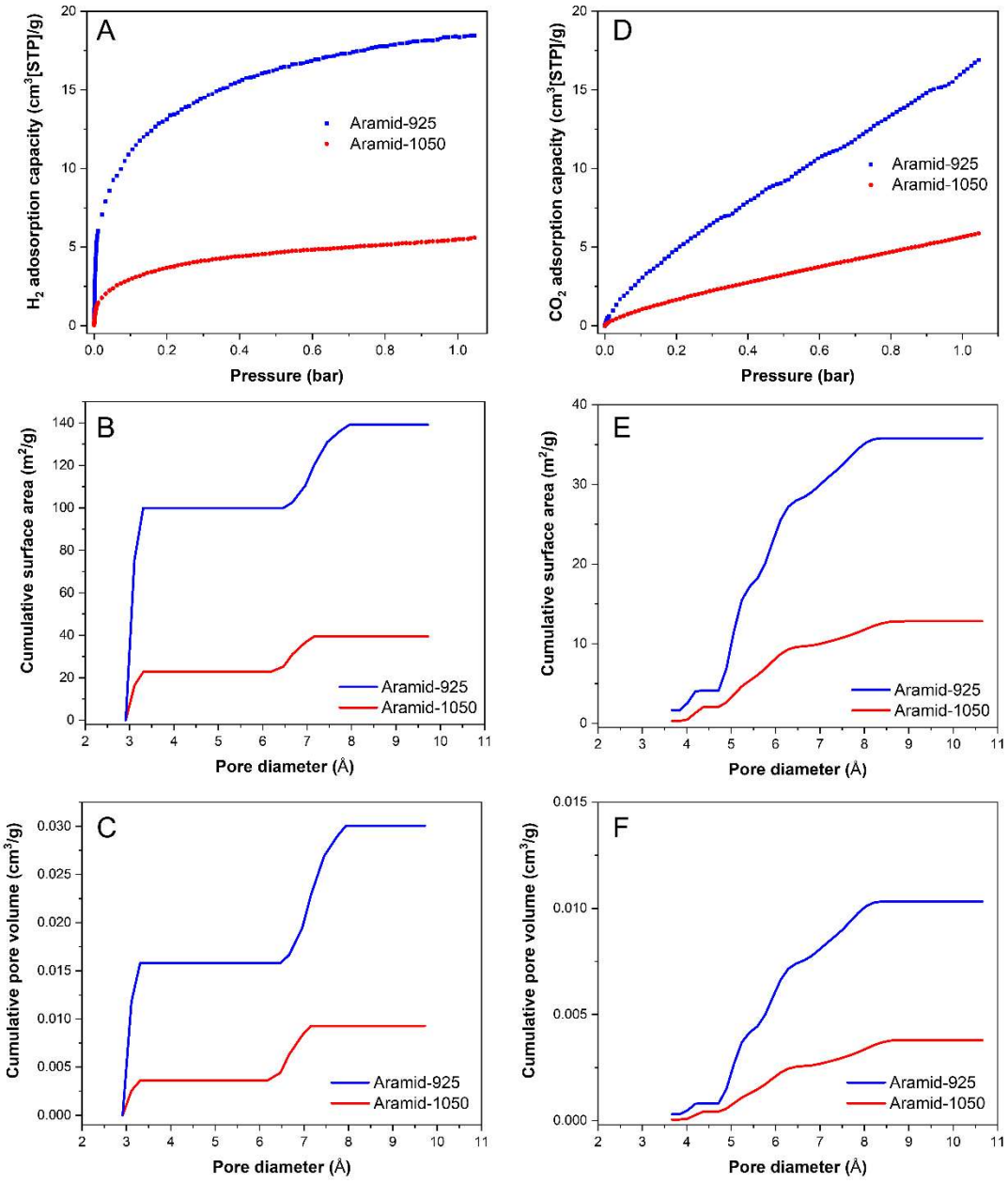


Fig. S7. Gas physisorption porosimetry results in the Aramid-1050 and Aramid-925 CMS membranes. (A) H_2 physisorption isotherms at 77K. (B) Cumulative surface area obtained from the H_2 physisorption isotherms. (C) Cumulative pore volume obtained from the H_2 physisorption isotherms. (D) CO_2 physisorption isotherms at 273.15K. (E) Cumulative surface area obtained from the CO_2 physisorption isotherms. (F) Cumulative pore volume obtained from the CO_2 physisorption isotherms.

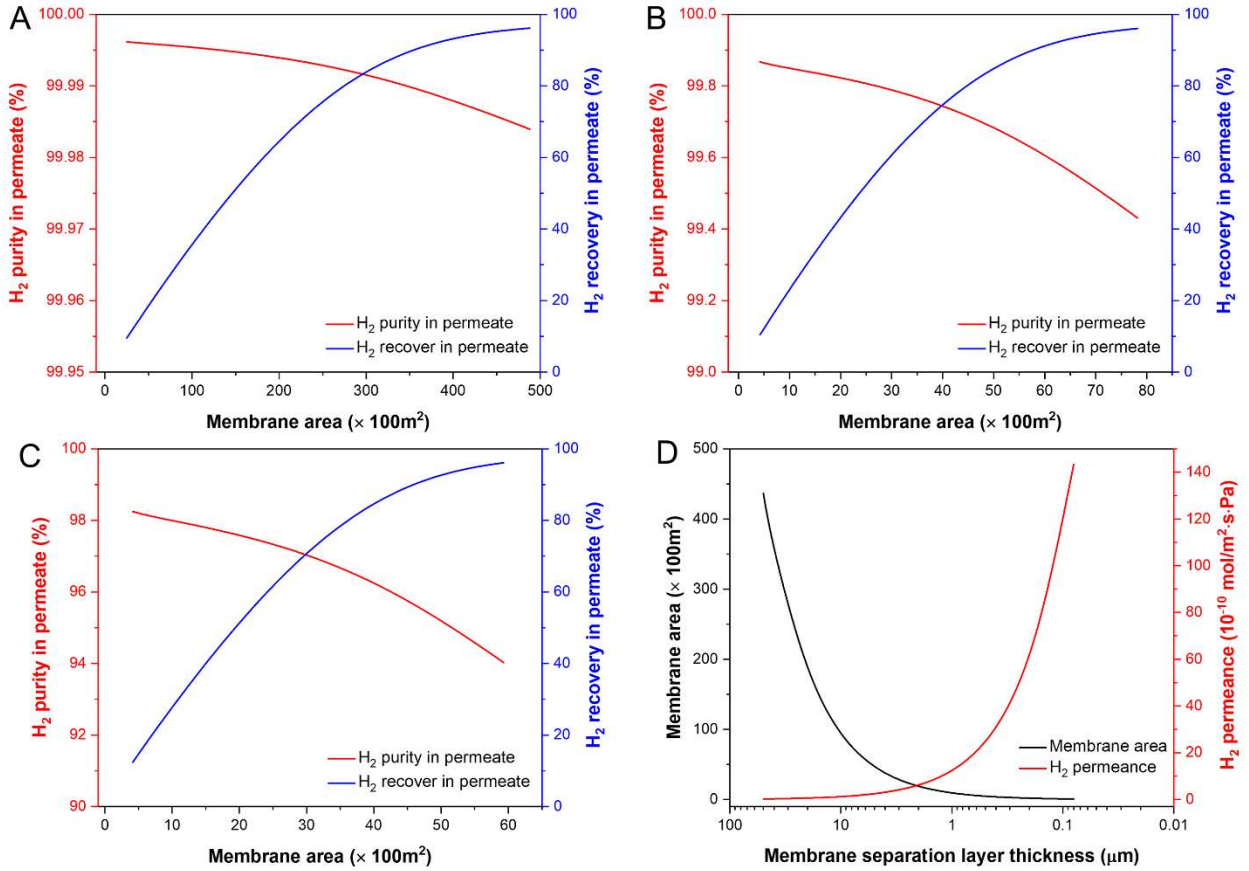


Fig. S8. Modeling results showing the effect of membrane area on H_2 purity and H_2 recovery in the permeate stream of a membrane separator that consists of (A) Aramid-1050 CMS membrane, (B) Aramid-925 CMS membrane, (C) PBI polymer membrane. (D) Modeling results showing the effect of membrane separation layer thickness on H_2 permeance of the Aramid-1050 CMS membrane and the required membrane area to produce a 99.99% H_2 permeate stream with 90% H_2 recovery.

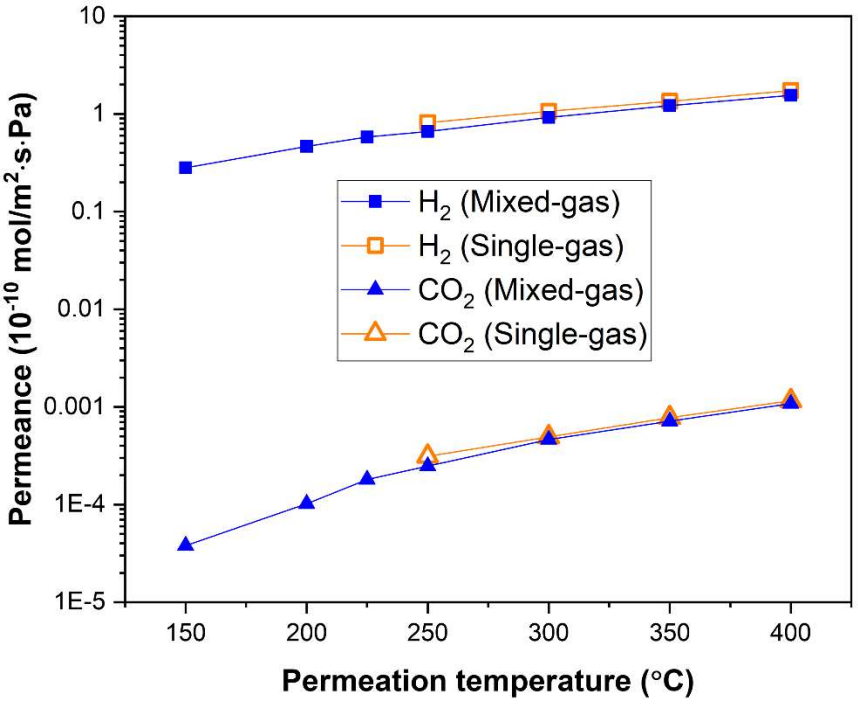


Fig. S9. The effect of permeation temperature on H_2 and CO_2 permeances of the Aramid-1050 CMS membrane (1 GPU = 3.348×10^{-10} mol/m^2·s·Pa).

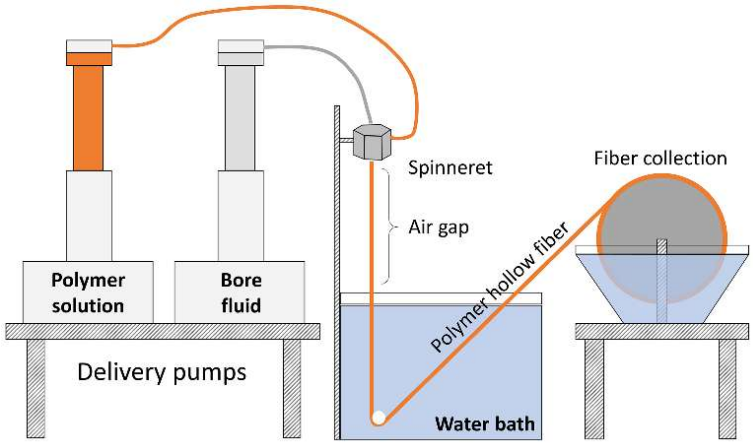


Fig. S10. Schematic illustrating the customized dry-jet/wet-quench spinning system used to fabricate the aramid precursor hollow fibers.(*14*)

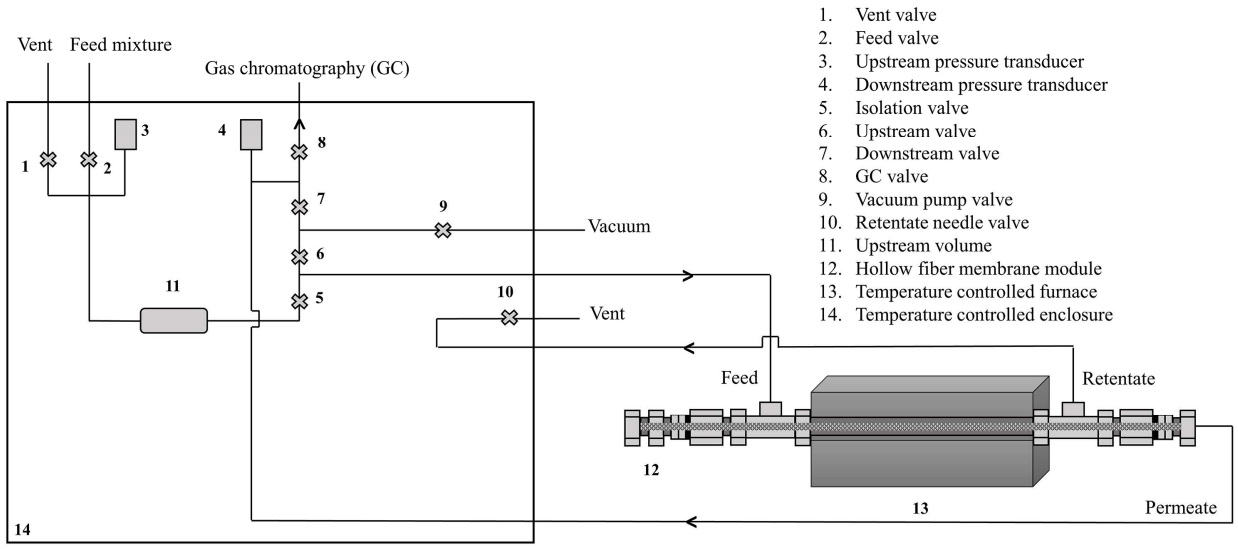


Fig. S11. Schematic illustrating the constant volume-variable pressure permeation system for high-temperature mixed-gas permeation measurements of the CMS hollow fiber membranes.

Table S1. Spinning dope composition and spinning conditions of the aramid precursor hollow fiber.

Spinning Conditions	Unit	Value
Dope composition	wt% Aramid	27
	wt% NMP	72
	wt% THF	1
Spinning temperature	°C	90
Lab relative humidity	%	58
Quench bath temperature	°C	50
Dope/bore fluid flow rate	cm^3/h	150/150
Bore fluid composition	NMP/H_2O	72/28
Air gap height	cm	3
Fiber take-up rate	m/min	10

Table S2. Summary of mixed-gas H_2/CO_2 separation performance (permeation at 100 °C and above) in CMS membranes and non-CMS inorganic membranes.

	Membrane	Permeation temperature (°C)	Feed pressure (bar)	Feed composition (mol%H_2/mol%CO_2)	H_2 permeability (Barrer)	H_2/CO_2 selectivity	Ref.
Non-CMS inorganic and hybrid	RUB-15	200	1	50/50	67	106	(*36*)
	SAPO-34	200	14	50/50	209	20	(*37*)
	ZIF/GO	250	1	50/50	388	14.9	(*38*)
	COF	150	1.2	50/50	2566	22.6	(*39*)
	GO	100	1	50/50	450	250	(*25*)
	Silica	200	1	50/50	1493	71	(*40*)
	2D $Zin_2(Bim)_3$	120	1	50/50	2400	166	(*41*)
	2D $Zin_2(Bim)_4$	200	1	50/50	5000	90	(*41*)
	POF	150	2	50/50	24.2	39.5	(*24*)
	JUC-150	200	1	50/50	452.4	30.2	(*42*)
CMS membranes	CANAL-900	100	2	50/50	9.8	256	(*15*)
	CANAL-900	100	10	50/50	8.2	174	(*15*)
	PBI-900	100	11	50/50	39	53	(*20*)
	PBI-PPA-600	150	6.5	50/50	116	33	(*43*)
	Aramid-925	100	2	10/90	12.6	169	This work
	Aramid-925	125	2	10/90	16.9	176	This work
	Aramid-925	150	2	10/90	20.7	200	This work
	Aramid-1050	150	2	10/90	3.4	7395	This work
	Aramid-1050	200	2	10/90	5.1	4565	This work
	Aramid-1050	225	2	10/90	6.3	3226	This work
	Aramid-1050	250	2	10/90	7.2	2677	This work
	Aramid-1050	250	5	10/90	7.2	2688	This work
	Aramid-1050	250	10	10/90	7.1	2743	This work
	Aramid-1050	250	15	10/90	6.8	2660	This work
	Aramid-1050	300	2	10/90	10	1988	This work
	Aramid-1050	350	2	10/90	14.9	1703	This work
	Aramid-1050	400	2	10/90	19	1437	This work
	Aramid-1050	400	2	50/50	20.5	1573	This work
	Aramid-1050	400	2	75/25	20.5	1605	This work

Table S3. Feed and permeate conditions for membrane separator modeling.

Parameter	**Value**
Feed molar composition	74.1%H_2/18.5%CO_2/6.9%CH_4/0.5%CO
Feed molar flow rate (mol/s)	1
Feed pressure (bar)	15
Permeate pressure (bar)	1
Permeation temperature (°C)	150

Table S4. Membrane properties for membrane separator modeling. It was assumed that all membranes were impermeable to CO and CH_4.

Parameter	Aramid-1050 CMS membrane	Aramid-925 CMS membrane	PBI polymer membrane
H_2 permeability (Barrer)	3.4	20.7	25
H_2/CO_2 selectivity	7395	200	15
Membrane separation layer thickness (μm)	41	41	41
H_2 permeance (mol/[m^2·s·Pa])	2.8×10^{-11}	1.67×10^{-10}	2.0×10^{-10}

Table S5. An example calculation of mixed-gas H_2/CO_2 separation performance of the Aramid-1050 CMS membrane. The mixed-gas permeation measurement was done using the constant volume-variable pressure method at a feed pressure of 2 bar and permeation temperature of 250 °C.

	Parameter	**Value**
Permeation conditions	Feed composition	10%H_2/90%CO_2
	Feed pressure (bar)	2
	Permeate pressure (bar)	0.013
	Temperature of membrane (°C)	250
	Downstream volume (cm^3)	34.75
Membrane properties	Membrane thickness (μm)	41
	Membrane area (cm^2)	10.1
Measurement results	Steady-state slope of permeation plot (torr/s)	7.5×10^{-4}
	Downstream leak rate (torr/s)	5.4×10^{-6}
	H_2 molar fraction in permeate (%)*	99.665
	CO_2 molar fraction in permeate (%)*	0.335
Calculation results	Total permeation flux (cm^3[STP]/s)	3.18×10^{-5}
	H_2 permeation flux (cm^3[STP]/s)	3.169×10^{-5}
	CO_2 permeation flux (cm^3[STP]/s)	1.065×10^{-7}
	H_2 permeance (10^{-10} mol/m^2·s·Pa)	0.588
	CO_2 permeance (10^{-10} mol/m^2·s·Pa)	2.2×10^{-4}
	H_2 permeability (Barrer)	7.2
	CO_2 permeability (Barrer)	0.00269
	H_2/CO_2 selectivity	2677

*Average value of three GC injections

REFERENCES AND NOTES

1. A. Boretti, B. K. Banik, Advances in hydrogen production from natural gas reforming. *Adv. Energy Sustainability Res.* **2**, 2100097 (2021).

2. N. W. Ockwig, T. M. Nenoff, Membranes for hydrogen separation. *Chem. Rev.* **107**, 4078–4110 (2007).

3. F. Dawood, M. Anda, G. M. Shafiullah, Hydrogen production for energy: An overview. *Int. J. Hydrogen Energy* **45**, 3847–3869 (2020).

4. M. Melaina, M. Penev, D. Heimiller, "Resource assessment for hydrogen production: Hydrogen production potential from fossil and renewable energy resources" (NREL/TP-5400-55626, NREL, 2013).

5. R. W. Baker, B. T. Low, Gas separation membrane materials: A perspective. *Macromolecules* **47**, 6999–7013 (2014).

6. D. F. Sanders, Z. P. Smith, R. Guo, L. M. Robeson, J. E. McGrath, D. R. Paul, B. D. Freeman, Energy-efficient polymeric gas separation membranes for a sustainable future: A review. *Polymer* **54**, 4729–4761 (2013).

7. Y. Han, W. S. W. Ho, Polymeric membranes for CO_2 separation and capture. *J. Membr. Sci.* **628**, 119244 (2021).

8. L. Liu, D. Liu, C. Zhang, High-temperature hydrogen/propane separations in asymmetric carbon molecular sieve hollow fiber membranes. *J. Membr. Sci.* **642**, 119978 (2022).

9. C. Zhang, G. B. Wenz, P. J. Williams, J. M. Mayne, G. Liu, W. J. Koros, Purification of aggressive supercritical natural gas using carbon molecular sieve hollow fiber membranes. *Ind. Eng. Chem. Res.* **56**, 10482–10490 (2017).

10. Z. Liu, W. Qiu, W. Quan, W. J. Koros, Advanced carbon molecular sieve membranes derived from molecularly engineered cross-linkable copolyimide for gas separations. *Nat. Mater.* **22**, 109–116 (2023).

11. T. Araújo, M. Andrade, G. Bernardo, A. Mendes, Stable cellulose-based carbon molecular sieve membranes with very high selectivities. *J. Membr. Sci.* **641**, 119852 (2022).

12. X. Ma, Y. S. Lin, X. Wei, J. Kniep, Ultrathin carbon molecular sieve membrane for propylene/propane separation. *AIChE J.* **62**, 491–499 (2016).

13. D.-Y. Koh, B. A. McCool, H. W. Deckman, R. P. Lively, Reverse osmosis molecular differentiation of organic liquids using carbon molecular sieve membranes. *Science* **353**, 804–807 (2016).

14. C. Zhang, R. Kumar, W. J. Koros, Ultra-thin skin carbon hollow fiber membranes for sustainable molecular separations. *AIChE J.* **65** e16611 (2019).

15. K. Hazazi, Y. Wang, N. M. S. Bettahalli, X. Ma, Y. Xia, I. Pinnau, Catalytic arene-norbornene annulation (CANAL) ladder polymer derived carbon membranes with unparalleled hydrogen/carbon dioxide size-sieving capability. *J. Membr. Sci.* **654**, 120548 (2022).

16. T. Merkel, "Novel polymer membrane process for pre-combustion CO2 capture from coal-fired syngas" (Membrane Technology and Research, Incorporated, 2011).

17. G. M. Iyer, C. Zhang, Precise hydrogen sieving by carbon molecular sieve membranes derived from solution-processable aromatic polyamides. *ACS Mater. Lett.* **5**, 243–248 (2023).

18. A. Garshasbi, H. Chen, M. Cao, S. Karagöz, R. J. Ciora, P. K. T. Liu, V. I. Manousiouthakis, T. T. Tsotsis, Membrane-based reactive separations for process intensification during power generation. *Catal. Today* **331**, 18–29 (2019).

19. L. Liu, A. Bhowmick, S. Cheng, B. H. Blazquez, Y. Pan J. Zhang, Y. Zhang Y. Shu, D. T. Tran, Y. Luo, M. Ierapetritou C. Zhang, D. Liu, Alkane dehydrogenation in scalable and electrifiable carbon membrane reactor. *Cell Rep. Phys. Sci.* **4**, 101692 (2023).

20. M. Omidvar, H. Nguyen, H. Liang, C. M. Doherty, A. J. Hill, C. M. Stafford, X. Feng, M. T. Swihart, H. Lin, Unexpectedly strong size-sieving ability in carbonized polybenzimidazole for membrane H_2/CO_2 separation. *ACS Appl. Mater. Interfaces* **11**, 47365–47372 (2019).

21. L. Xu, M. Rungta, J. Hessler, W. Qiu, M. Brayden, M. Martinez, G. Barbay, W. J. Koros, Physical aging in carbon molecular sieve membranes. *Carbon* **80**, 155–166 (2014).

22. G. M. Iyer, C.-E. Ku, C. Zhang, Polyamide-imide copolymer-derived carbon molecular sieve membranes for efficient hydrogen/carbon dioxide separation. *Carbon* **216**, 118598 (2024).

23. L. Lei, F. Pan, A. Lindbråthen, X. Zhang, M. Hillestad, Y. Nie, L. Bai, X. He, M. D. Guiver, Carbon hollow fiber membranes for a molecular sieve with precise-cutoff ultramicropores for superior hydrogen separation. *Nat. Commun.* **12**, 268 (2021).

24. M. Shan, X. Liu, X. Wang, I. Yarulina, B. Seoane, F. Kapteijn, J. Gascon, Facile manufacture of porous organic framework membranes for precombustion CO_2 capture. *Sci. Adv.* **4** eaau1698 (2018).

25. H. Li, Z. Song, X. Zhang, Y. Huang, S. Li, Y. Mao, H. J. Ploehn, Y. Bao, M. Yu, Ultrathin, molecular-sieving graphene oxide membranes for selective hydrogen separation. *Science* **342**, 95–98 (2013).

26. C. Zhang, W. J. Koros, Ultraselective carbon molecular sieve membranes with tailored synergistic sorption selective properties. *Adv. Mater.* **29**, 1701631 (2017).

27. W. Qiu, J. E. Leisen, Z. Liu, W. Quan, W. J. Koros, Key features of polyimide-derived carbon molecular sieves. *Angew. Chem. Int. Ed.* **60**, 22322–22331 (2021).

28. J. Jagiello, A. Ansón, M. T. Martínez, DFT-based prediction of high-pressure H_2 adsorption on porous carbons at ambient temperatures from low-pressure adsorption data measured at 77 K. *J. Phys. Chem. B* **110**, 4531–4534 (2006).

29. R. W. Baker, K. Lokhandwala, Natural gas processing with membranes: An overview. *Ind. Eng. Chem. Res.* **47**, 2109–2121 (2008).

30. Z. Ali, F. Pacheco, E. Litwiller, Y. Wang, Y. Han, I. Pinnau, Ultra-selective defect-free interfacially polymerized molecular sieve thin-film composite membranes for H_2 purification. *J. Mater. Chem. A* **6**, 30–35 (2018).

31. M. Luberti, H. Ahn, Review of polybed pressure swing adsorption for hydrogen purification. *Int. J. Hydrogen Energy* **47**, 10911–10933 (2022).

32. T. C. Merkel, H. Lin, X. Wei, R. Baker, Power plant post-combustion carbon dioxide capture: An opportunity for membranes. *J. Membr. Sci.* **359**, 126–139 (2010).

33. M. Y. Jeon, D. Kim, P. Kumar, P. S. Lee, N. Rangnekar, P. Bai, M. Shete, B. Elyassi, H. S. Lee, K. Narasimharao, S. N. Basahel, S. Al-Thabaiti, W. Xu, H. J. Cho, E. O. Fetisov, R. Thyagarajan, R. F. DeJaco, W. Fan, K. A. Mkhoyan, J. I. Siepmann, M. Tsapatsis, Ultra-selective high-flux membranes from directly synthesized zeolite nanosheets. *Nature* **543**, 690–694 (2017).

34. M. R. Kosuri, W. J. Koros, Defect-free asymmetric hollow fiber membranes from Torlon®, a polyamide–imide polymer, for high-pressure CO_2 separations. *J. Membr. Sci.* **320**, 65–72 (2008).

35. D. Q. Vu, W. J. Koros, S. J. Miller, High pressure CO_2/CH_4 separation using carbon molecular sieve hollow fiber membranes. *Ind. Eng. Chem. Res.* **41**, 367–380 (2002).

36. M. Dakhchoune, L. F. Villalobos, R. Semino, L. Liu, M. Rezaei, P. Schouwink, C. E. Avalos, P. Baade, V. Wood, Y. Han, M. Ceriotti, K. V. Agrawal, Gas-sieving zeolitic membranes fabricated by condensation of precursor nanosheets. *Nat. Mater.* **20**, 362–369 (2021).

37. M. Yu, H. H. Funke, R. D. Noble, J. L. Falconer, H_2 separation using defect-free, inorganic composite membranes. *J. Am. Chem. Soc.* **133**, 1748–1750 (2011).

38. A. Huang, Q. Liu, N. Wang, Y. Zhu, J. Caro, Bicontinuous zeolitic imidazolate framework ZIF-8@GO membrane with enhanced hydrogen selectivity. *J. Am. Chem. Soc.* **136**, 14686–14689 (2014).

39. Y. Ying, M. Tong, S. Ning, S. K. Ravi, S. B. Peh, S. C. Tan, S. J. Pennycook, D. Zhao, Ultrathin two-dimensional membranes assembled by ionic covalent organic nanosheets with reduced apertures for gas separation. *J. Am. Chem. Soc.* **142**, 4472–4480 (2020).

40. R. M. de Vos, H. Verweij, High-selectivity, high-flux silica membranes for gas separation. *Science* **279**, 1710–1711 (1998).

41. Y. Peng, Y. Li, Y. Ban, W. Yang, Two-dimensional metal–organic framework nanosheets for membrane-based gas separation. *Angew. Chem. Int. Ed.* **56**, 9757–9761 (2017).

42. Z. Kang, M. Xue, L. Fan, L. Huang, L. Guo, G. Wei, B. Chen, S. Qiu, Highly selective sieving of small gas molecules by using an ultra-microporous metal–organic framework membrane. *Energ. Environ. Sci.* **7**, 4053–4060 (2014).

43. L. Hu, V. T. Bui, A. Krishnamurthy, S. Fan, W. Guo, S. Pal, X. Chen, G. Zhang, Y. Ding, R. P. Singh, M. Lupion, H. Lin, Tailoring sub-3.3 Å ultramicropores in advanced carbon molecular sieve membranes for blue hydrogen production. *Sci. Adv.* **8** eabl8160 (2022).